Available online at www.sciencedirect.com
ScienceDirect
International Journal of Heat and Fluid Flow 29 (2008) 733–742
International Journal of HEAT AND FLUID FLOW
www.elsevier.com/locate/ijhff

Dispersion of a vertical jet of buoyant particles in a stably stratified wind-driven Ekman layer

R. Inghilesi [a], V. Stocca [b], F. Roman [b], V. Armenio [b,*]

[a] Dipartimento Tutela delle Acque Interne e Marine, APAT Via Vitaliano Brancati 48, 00144 Roma, Italy
[b] Dipartimento di Ingegneria Civile e Ambientale, Università di Trieste, Piazzale Europa 1, 34127 Trieste, Italy

Received 10 November 2007; received in revised form 3 February 2008; accepted 9 February 2008
Available online 1 April 2008

Abstract

Dispersion of a buoyant jet of particles (i.e. fresh water) in a salt water thermally stratified environment is investigated. The carrying flow field is a wind-driven mid-latitude Ekman layer. The investigation is carried out using Large Eddy Simulation. The dispersed phase is simulated in a Lagrangian way, solving a modified form of the Maxey and Riley equation for each particle of the jet. In order to simulate a large Reynolds number flow, the thin wall layer is not directly resolved and the wall stress and the wall heat flux are directly imposed at the free surface. Results of the simulations show that the presence of incoming heat flux produces a thin region of large density gradients below the free surface and inhibits turbulent transport. In particular, the turbulent penetration depth is strongly reduced by stratification as well as the level of the turbulent fluctuations. In order to consider the effect of the actual density field on the particle dynamics, an improved version of the particle-motion equation is here proposed. The results of our simulations show that the dispersion of the buoyant plume of particles is dramatically modified by stratification. In the neutral case, the plume is spread over the horizontal direction in the free surface region and is driven by the mean Ekman current. In the stratified case, the particles remain entrapped in wavy motion present in the region of large mean density gradients. The horizontal transport is strongly reduced for two reasons: first in the region where large density gradients develop the mean velocity is small compared with the value reached at the free surface; second, the turbulent transport is very small due to the suppression of velocity fluctuations. Finally, our results show that very inaccurate predictions are obtained if the variation of density due to the vertical stratification is not taken into account in the particle motion equation.

Keywords: LES; Ekman layer; Stable stratification; Particle dispersion

1. Introduction

An environmental problem that is becoming increasingly relevant nowadays is the prediction of dispersion of polluting particulate in a marine environment. Particles of buoyant fluid in a marine environment may be released for example when leakage occurs in submarine pipelines or other devices (oil spilling problems). In this kind of applications it is of significant interest the evaluation of the concentration of the released substance as well as the evaluation of the amount of particulate that reaches the free surface of the sea. In literature (see for example Rubin and Atkinson (2001) for a general discussion) Eulerian models are commonly used, in which the plume of particles is described in an Eulerian way as a space-time distribution of their concentration. Although this approach is computationally inexpensive, it suffers from empiricism in particular when the concentration of the dispersed phase is small and it is mainly composed of an ensemble of separate particles traveling in the carrying fluid. In the present paper we study the dispersion of a buoyant jet of particles released into a salty water basin. Note that since the time scale of diffusion of salinity is usually much larger than the buoyancy time scale, this analysis can also be applied to upwelling of fresh water particles in a salty water ambient.

* Corresponding author. Tel.: +39 040 5583472; fax: +39 040 572082.
E-mail address: armenio@dica.units.it (V. Armenio).

0142-727X/$ - see front matter © 2008 Elsevier Inc. All rights reserved.
doi:10.1016/j.ijheatfluidflow.2008.02.004

In particular, we study an archetypal problem, representative of the upper part of the ocean forced by a constant wind stress and the release of the buoyant particles in a region below the free surface where turbulent mixing is negligible.

From a fundamental point of view, the top region of the sea can be treated as a wind-driven Ekman layer, namely the boundary layer created by the tangential stress supplied by the action of the wind in a rotating environment. The Coriolis force causes a rotation of the velocity profiles and thus generates a component in the spanwise direction. In laminar conditions the penetration depth of the Ekman layer (the thickness on the boundary layer) is proportional to $\sqrt{2\nu/f_z}$ (the z-direction is vertical upward) where ν is the fluid viscosity and f_z is the Coriolis parameter. In the turbulent regime the penetration depth is found to be proportional to u_τ/f_z where $u_\tau = \sqrt{\tau_w/\rho_0}$ is the friction velocity associated to the free surface wind stress τ_w, and ρ_0 is the reference density of the water. A detailed discussion on the Ekman layer and its relevance in environmental fluid mechanics is in Price and Sundermeyer (1999). The main scope the present work is to understand how a cloud of buoyant particles released in the water column is dispersed in the wind-driven Ekman layer subject to different conditions of thermal stratification. To this aim an extension of the Maxey and Riley equation (Maxey and Riley, 1983) for the particle motion is proposed, which takes into account the actual fluid density during the space-time evolution of the particle swarm. The study is performed numerically using a Lagrangian–Eulerian approach, which consists of moving Lagrangian particles in an Eulerian carrier phase. The paper is organized as follows: Section 2 contains a description of the problem investigated together with the mathematical formulation. Specifically the new form of the particle-motion equation is presented and discussed. In Section 3 the results of the simulations are discussed and concluding remarks are given in Section 4.

2. The problem formulation

We use a Lagrangian–Eulerian approach, in which the dispersed phase is treated as an ensemble of Lagrangian particles moving in an Eulerian flow field. In order to evaluate the force field acting over the Lagrangian particles an interpolation of the Eulerian flow field onto the particle position is carried out. A detailed description of the mathematical method is here supplied.

2.1. The Eulerian field

We consider a mid-latitude, wind-driven Ekman layer, thus including both the vertical and the horizontal components of the rotation vector in the governing equations (see Coleman et al. (1990) and Salon et al. (2005)). The relevant scales of the problem are: the already defined friction velocity u_τ, the time scale $T = 1/f_z$ associated to the Coriolis parameter and the penetration length $\delta = u_\tau/f_z$ which gives an estimation of the depth of the turbulent boundary layer. The stratification is considered as a variation of the density field with respect to a reference value ρ_0. Specifically the density field is $\rho_{\mathrm{tot,d}}(x,y,z,t) = \rho_0 + \rho_\mathrm{d}(x,y,z,t)$ with $\rho_\mathrm{d} \ll \rho_0$ (hereafter the index d denotes dimensional quantities). In our numerical experiment the stratification comes from the imposition of a heat flux at the free surface, as in Taylor et al. (2005); physically this corresponds to heating a fluid column by an incoming heat flux. Here we discuss two cases, respectively the case of neutral flow $Ri \to 0$ and the case of strongly stratified flow $Ri = 40$ where the Richardson number is $Ri = g/\rho_0 |\mathrm{d}\rho/\mathrm{d}z|_{fs} \delta^2/u_\tau^2$. In the present case, the Richardson number is defined using a density scale $|\mathrm{d}\rho/\mathrm{d}z|_{fs}|\delta$ which is related to the free surface heat flux as follows $\mathrm{d}\rho/\mathrm{d}z|_{fs} = -\rho_0 \alpha \mathrm{d}T/\mathrm{d}z|_{fs}$, with α the thermal expansion coefficient. The wind stress acts in the direction south-north (x axis), the y-axis is directed from east to west and the z-axis is vertical upward. A mid-latitude case ($\theta = 45^\circ$ where θ is the latitude) is here considered: with the frame of reference herein used, the components of the rotation vector are the vertical one $f_z = 2\Omega_H \sin\theta$ and the horizontal one $f_x = 2\Omega_H \cos\theta$ where Ω_H is the earth rotation frequency. A typical full-scale value of $Re = u_\tau \delta/\nu$ is of the order of 7×10^5 considering the data of wind stress given in Price and Sundermeyer (1999). Although the approach we use, equivalent to that employed in the $Re \to \infty$ simulation of Zikanov et al. (2003), can deal with applicative values of the Reynolds number, here we consider a moderate value of Reynolds number $Re = 10,000$ (see Section 2.3). This value of Re is such to minimize Reynolds number effects on the dynamics of the flow field.

The equations of the Eulerian flow are solved using Large Eddy Simulation (LES). We use the Boussinesq approximation which holds in cases where the density variations in the flow field are small compared to a reference density ρ_0. This approximation is commonly used in the analysis of thermally stratified water. In the present paper directions 1, 2, 3, respectively correspond to x, y, z. The non-dimensional filtered equations are:

$$\frac{\partial \bar{u}_i}{\partial x_i} = 0 \tag{1}$$

$$\frac{\partial \bar{u}_i}{\partial t} + \frac{\partial \bar{u}_j \bar{u}_i}{\partial x_j} = -\frac{\partial \bar{p}}{\partial x_i} + \frac{1}{Re}\frac{\partial^2 \bar{u}_i}{\partial x_j \partial x_j} - \epsilon_{ijk}\frac{f_j}{|f_3|}\bar{u}_k - Ri\bar{\rho}\delta_{i3} - \frac{\partial \tau_{ij}}{\partial x_j} \tag{2}$$

$$\frac{\partial \bar{\rho}}{\partial t} + \frac{\partial \bar{u}_j \bar{\rho}}{\partial x_j} = \frac{1}{RePr}\frac{\partial^2 \bar{\rho}}{\partial x_j \partial x_j} - \frac{\partial \lambda_i}{\partial x_i} \tag{3}$$

where the symbol $\bar{\cdot}$ denotes a filtering operation. In Eqs. (1) and (2) t is time made non-dimensional with $1/f_z$, u_i is the velocity component in the i-direction made non-dimensional with u_τ, x_i is the i-coordinate made non-dimensional with δ, p is the pressure made non dimensional with $\rho_0 u_\tau^2 = \tau_w$, and ρ is the density made non-dimensional with the density scale $\delta|\mathrm{d}\rho/\mathrm{d}z|_{fs}|$. The non-dimensional groups

Re and Ri have been already defined, the Prandtl number is $Pr = \nu/k$ with k the thermal diffusivity of the medium.

The quantities $\tau_{ij} = \overline{u_i u_j} - \bar{u}_i \bar{u}_j$ and $\lambda_i = \overline{u_i \rho} - \bar{u}_i \bar{\rho}$ are, respectively the subgrid-scale (SGS) stresses and the SGS buoyancy fluxes. Here we use a dynamic-mixed model for the SGS momentum fluxes, composed of a scale-similar part (Bardina et al., 1980) and an eddy viscosity one:

$$\tau_{ij} = (\overline{\bar{u}_i \bar{u}_j} - \bar{\bar{u}}_i \bar{\bar{u}}_j) - 2C\overline{\Delta}^2 |\overline{S}| \overline{S}_{ij} \tag{4}$$

In Eq. (4) the first parenthesis on the right hand side is the scale-similar part, C is the constant, $\bar{\Delta}$ is the filter width, $\overline{S}_{ij}$ is the resolved strain rate tensor and $|\overline{S}|$ is its contraction. The SGS density fluxes are parametrized using a dynamic eddy diffusivity model:

$$\lambda_i = -C_\rho \overline{\Delta}^2 |S| \frac{\partial \bar{\rho}}{\partial x_i} \tag{5}$$

In Eqs. (4) and (5) the constants C and C_ρ are calculated dynamically, as described with details in Armenio and Sarkar (2002). Specifically the authors have extensively shown that such a model is able to adjust automatically to the actual flow conditions and to predict the superlinear behavior of the SGS Prandtl number ($Pr_{\mathrm{SGS}} = \nu_{\mathrm{sgs}}/k_{\mathrm{sgs}}$) which, as well known in literature, occurs in strongly stably stratified turbulence.

2.2. The Lagrangian phase

The dispersed phase is treated in a Lagrangian way using a simplified form of the Maxey and Riley equation (see Maxey and Riley (1983)). Following Armenio and Fiorotto (2001) the Stokes drag is considered in the particle motion equation together with the gravity term. In the present work we consider the effect of the variation of density of the Eulerian field in the particle motion equation. A description of the proposed modification is given here.

The dimensional equation of the particle motion is:

$$\frac{\mathrm{d}V_{\mathrm{p},i}}{\mathrm{d}t_{\mathrm{d}}} = \left(\frac{\rho_{\mathrm{p}} - \rho_{\mathrm{tot,d}}}{\rho_{\mathrm{p}}}\right) g\delta_{i3} + \frac{3}{4D_{\mathrm{p}}} C_{\mathrm{D}} |U_{\mathrm{p},i} - V_{\mathrm{p},i}| (U_{\mathrm{p},i} - V_{\mathrm{p},i}) - 2\epsilon_{ijk}\Omega_j V_{p,k} \tag{6}$$

In Eq. (6) t_{d} is the dimensional time, $V_{\mathrm{p},i}$ and $U_{\mathrm{p},i}$ are, respectively are the i-component of the dimensional particle velocity and of the dimensional fluid velocity at the particle location, ρ_{p} and D_{p} are, respectively the density and the diameter of the particle, $C_{\mathrm{D}} = 24/Re_{\mathrm{p}}(1 + 0.15Re_{\mathrm{p}}^{0.687})$ where $Re_{\mathrm{p}} = |U_{\mathrm{p},i} - V_{\mathrm{p},i}| D_{\mathrm{p}}/\nu$ is the particle Reynolds number. If we replace the total density $\rho_{\mathrm{tot,d}}$ with $\rho_0 + \rho_{\mathrm{d}}$, and we make Eq. (6) non-dimensional we obtain:

$$\frac{\mathrm{d}v_{\mathrm{p},i}}{\mathrm{d}t} = \left(1 - \frac{1}{\Delta\rho}\right) \frac{1}{Fr^2} \delta_{i3} - \frac{Ri}{\Delta\rho} \rho \delta_{i3} + \frac{3}{4d_{\mathrm{p}}} C_{\mathrm{D}} |u_{\mathrm{p},i} - v_{\mathrm{p},i}| (u_{\mathrm{p},i} - v_{\mathrm{p},i}) - \epsilon_{ijk} \frac{\Omega_j}{\Omega_3} v_{p,k} \tag{7}$$

In Eq. (7) $\Delta\rho = \rho_{\mathrm{p}}/\rho_0$, $v_{\mathrm{p},i} = V_{\mathrm{p},i}/u_\tau$, $u_{\mathrm{p},i} = U_{\mathrm{p},i}/u_\tau$, $d_{\mathrm{p}} = D_{\mathrm{p}}/\delta$ and the buoyancy contribution appears split into two terms: the first one is the usual contribution proportional to the Froude number $Fr = u_\tau/(g\delta)^{0.5}$; the second one takes into account the density variation in the Eulerian field, and is proportional to the Richardson number. Note that $Fr^2 Ri = \rho_{\mathrm{s}}/\rho_0$ where ρ_{s} is a typical density scale of the problem under investigation, *i.e.* $\delta|\mathrm{d}\rho/\mathrm{d}z|_{fs}|$ in our case, thus $Fr^2 Ri \ll 1$ under the Boussinesq approximation. The second term (II) on the RHS of Eq. (7) gets important when it is comparable with the first term (I) on the RHS. It can be easily shown that $\mathrm{II}/\mathrm{I} = (\rho_{\mathrm{s}}/\rho_0)/((\rho_{\mathrm{p}} - \rho_0)/\rho_0)$, thus II influences the particle motion when the particle density is very similar to the reference density of the carrying fluid. This is the case, for instance, of particles of fresh water released in a salty water environment.

Finally the position of the particles is advanced in time as follows:

$$\frac{\mathrm{d}x_{\mathrm{p},i}}{\mathrm{d}t} = v_{\mathrm{p},i} \tag{8}$$

with $x_{\mathrm{p},i}$ the i-component of the particle position made non dimensional with δ.

2.3. The numerical method

The Lagrangian–Eulerian model herein employed works as follows: The LES field is first obtained through integration of the filtered Eqs. (1)–(3). Such integration is carried out using the fractional-step technique of Zang et al. (1994). Specifically, the advective and volume force terms are advanced in time explicitly using the Adams–Bashforth method, the diffusive terms are advanced in time implicitly using the Crank–Nicolson scheme; second-order centered derivatives are used for the discretization of the spatial derivatives. The Poisson equation for the pressure field is solved using a SOR iterative technique in conjunction with a V-cycle multigrid method. Details on the algorithm are in Zang et al. (1994) and are not repeated here.

Since the LES field does not contain the energy and vorticity contribution associated to the unresolved (small) scales of the motion, a SGS model for the motion of the Lagrangian particles is required. Note that in *resolved*-LES (simulations where the viscous sub-layer is directly resolved and consequently carried out at small values of the Reynolds number), it was shown that the contribution of the small unresolved scales of motion on particle dispersion is small and the error in the dispersion coefficients is proportional to the dissipation rate of the SGS turbulent scales (Armenio et al., 1999). On the other hand, when dealing with large values of the Reynolds number (that requires the use of a wall-layer model for the evaluation of the Eulerian field) neglecting the contribution of the small scales to the Lagrangian motion can lead to severe underestimation of the dispersion of the particle swarm. Since we simulate a large Reynolds number flow, in order to overcome this problem the LES field is then reconstructed

with the aim to recover the energy contribution associated to the unresolved scales. We use the approximate deconvolution technique recently applied by Kuerten (2006) and Shotorban and Mashayek (2005) to the problem of particle dispersion. Specifically, the following approximate deconvolution:

$$u_{r,i} = \bar{u}_i + (\bar{u}_i - \bar{\bar{u}}_i) + \left(\bar{u}_i - 2\bar{\bar{u}}_i + \bar{\bar{\bar{u}}}_i\right) + \cdots \tag{9}$$

when used in conjunction with an equivalent model for the SGS turbulent stresses was proven to be able to recover the SGS turbulent contribution to the particle motion. In Eq. (9) $u_{r,i}$ is the re-constructed i-component of the velocity field. Successive tests have shown that a first order re-construction (first two terms on the right hand side, RHS, of Eq. (9)) gives accurate results when used in conjunction with a dynamic-mixed model (Lupieri and Armenio, 2005). The reconstructed field is later on interpolated onto the particle position using a technique recently developed by Marchioli et al. (2007). This technique uses a Taylor expansion around the grid point (N) closest to the particle, to interpolate the Eulerian field onto the particle position (P):

$$u_{P,i} = u_{N,i} + \frac{\partial u_i}{\partial x_i}(x_{P,i} - x_{N,i}) + \mathrm{O}(\Delta x^2) \tag{10}$$

This technique is very simple and inexpensive, and allows obtaining second-order space-accuracy, as that achieved in the solution of the Eulerian field. The interpolated velocity is finally considered in the particle motion equation (Eq. (7)) and the particle position is thus advanced in time using a second-order accurate Adams–Bashforth technique.

As regards the Eulerian field, the mathematical model herein employed has been validated in a number of flow conditions (see among the others Armenio and Piomelli (2000), Armenio and Sarkar (2002), Salon et al. (2007)). Results of validation tests for the wind-driven Ekman layer are discussed in Section 3.1.

As regards the Lagrangian phase a direct comparison between our results and reference data is not possible, since, to the best of our knowledge, similar simulations are not available in literature. However, for values of Reynolds number smaller than that used in the present work, the accuracy of the Lagrangian–Eulerian model has been verified in the contest of an international test-case aimed at the validation of Lagrangian–Eulerian (LES) solvers (see the webpage http://www.wtb.tue.nl/woc/ptc/benchmark.pdf). Details on the validation tests are in Lupieri and Armenio (2005). Although the mathematical method is expected to work satisfactorily at values of Re larger than those used in the international test-case, we cannot guarantee that the SGS re-construction is still valid in the limiting case $Re \to \infty$, namely the value of Re employed in the wind-driven Ekman layer of Zikanov et al. (2003). The scope of the present paper is not the validation of the re-construction of the SGS field for the Lagrangian phase in the limiting case $Re \to \infty$, rather we are interested, first in the improvement of the particle-motion equation for the variable-density case and, second, to the analysis of the dispersion of the buoyant jet of particles. Thus we have decided to limit the Reynolds number of the simulation to a finite value, $Re = 10,000$, large enough to minimize Reynolds number effects on the flow dynamics and, at the same time, such to expect a reliable behavior from the SGS re-construction discussed in Kuerten (2006) and Shotorban and Mashayek (2005).

2.4. Computational parameters

Following Zikanov et al. (2003) the simulations are carried out over a rectangular box whose non-dimensional extensions are $L_x = 1$ and $L_y = 1$ in the horizontal directions, whereas $L_z = 1.5$. The domain size is large enough to reproduce the largest scales of motion both in the neutral case and in the stably stratified one. This occurs because stable stratification inhibits and destroys the largest scales of motion. The computational grid is uniform and has $64 \times 64 \times 200$ cells, respectively in the x, y and z directions. The grid spacing in wall units (made non-dimensional with ν/u_τ) is $\Delta x^+ = \Delta y^+ = 156$ and $\Delta z^+ = 75$. Such a grid size is typical of LES with wall-layer models (see Balaras et al. (1995)) and is also suited for stably stratified flows when dynamic SGS models are employed, due to the ability of the model constants to adapt to the actual flow conditions. The molecular Prandtl number is chosen equal to 5 which corresponds to thermally stratified water. Periodic boundary conditions are imposed over the horizontal directions, whereas at the bottom boundary of the computational domain we set $\rho = u_3 = \partial u_1/\partial x_3 = \partial u_2/\partial x_3 = 0$. This choice is justified by the fact that the domain depth is much larger than the turbulent penetration length and modifications of the flow variables are not expected at the bottom boundary. The *a posteriori* analysis of the numerical results confirmed the effectiveness of such a choice. We consider two cases, a case of neutral flow ($Ri \to 0$) and a case of stable stratified flow ($Ri = 40$). As we will discuss later in the paper, the latter corresponds to a case of strong stratification. In both cases, a statistically steady state is first obtained, and later on the particles are released. In the two cases analyzed, we have released 54,000 buoyant particles, with density ratio $\Delta\rho = \rho_p/\rho_0 = 0.976$, corresponding to fresh water particles released in a salt water environment and radius equal to $10^{-3}\delta$. The vertical plume is released continuously in time, up to $t = 1.1$, from a disc of radius 0.05δ, located at 0.5δ below the free surface and containing 900 particles. The particles have non zero initial vertical velocity $v_{p,3} = u_\tau$. As regards the choice of the parameters for the dispersed phase, the vertical location of the ejection disc was chosen in a turbulence-free region, close to the free surface in order to reduce the time needed to the particles to rise up to the surface. The radius of the disc was such to spread the particles over a number of grid cells and the choice of the initial velocity was made for having a typical velocity scale of the flow field. However tests have demonstrated that the

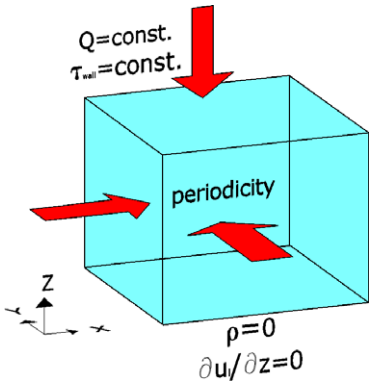

Fig. 1. Schematic of the physical problem herein investigated. The quantity Q denotes the free surface heat flux.

memory effect of the initial velocity is lost after a short time, and the physics ruling the rise of the particles is mainly associated to buoyancy effects. Finally the number of the particles was such to ensure that all the particles left the disc at the final time of the simulation.

A sketch of the problem herein discussed is in Fig. 1.

3. Results

First we discuss the results of the validation tests for the case under investigation, successively we show the statistics of the Eulerian field and finally we show the results of the Lagrangian phase.

3.1. Validation tests

To the best of our knowledge data of the wind-driven Ekman layer at $Re = 10,000$ are not available. The only results available for the problem under investigation are those of the polar $(f_x = f_y = 0)$ $Re \to \infty$ simulation of Zikanov et al. (2003). We have thus run a polar simulation at $Re = 10,000$ and compared our first- and second-order statistics with the reference data. Although the difference in the value of Re, the agreement between our results and the reference ones is pretty good, due to the fact that our Re number is large enough to minimize its own effect on the re-scaled velocity field. Fig. 2a shows the comparison of the vertical profile of the mean horizontal velocity components. The notation $\langle\cdot\rangle$ denotes Reynolds averaged quantities. Small differences are detectable in the outer region, well below the free surface. Specifically, as expected, the comparison shows a larger penetration depth in the $Re \to \infty$ case with respect to the moderate Reynolds number case. This difference has to be attributed to the fact that our finite Re number implies a smaller penetration depth than the one observable at $Re = \infty$. In Fig. 2b the comparison of the rms of the three velocity components is shown. As for the mean velocity components, they are very close to each other at the upper surface while some differences are observable in the outer region. This is a Reynolds number effect well known in literature, namely the normal Reynolds stresses do not scale with the friction velocity far from the wall and, when they are made non-dimensional with wall variables they slightly increase with Re.

3.2. The Eulerian field

Here, we discuss the results of the mid-latitude simulations in the two cases of stratification. Fig. 3a shows the vertical profiles of the horizontal components of the mean velocity field in the two cases analyzed. In the neutral case the penetration length of the turbulent field is of the order of δ and, as expected, large gradients are present in the free surface region. The transversal velocity arising from the rotational motion is large and negative in the free surface region, indicating a rotation of the velocity vector toward the right direction as expected in the northern hemisphere. In the stratified case, the velocity profiles are dramatically affected by the presence of large incoming free surface heat flux. In the stratified case (Fig. 3a) we observe a strong reduction of the penetration length of the boundary layer, a small increase of the streamwise velocity at the free surface and a noticeable increase of the spanwise component.

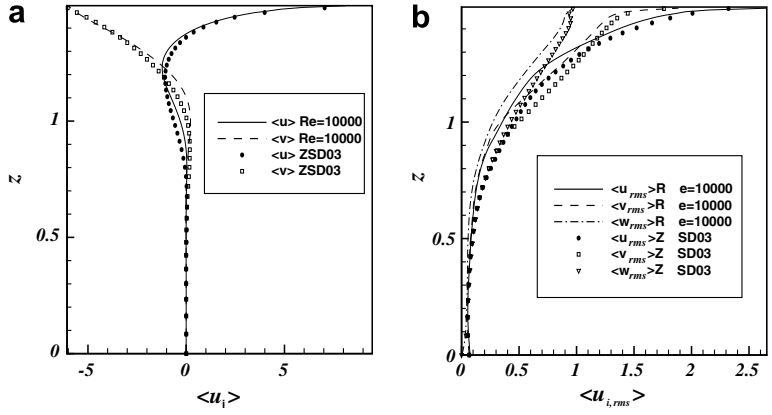

Fig. 2. Comparison of a polar $Re = 10,000$ simulation with the reference data of Zikanov et al. (2003) at $Re \to \infty$: (a) vertical profiles of the mean horizontal velocity components and (b) vertical profiles of the rms velocities.

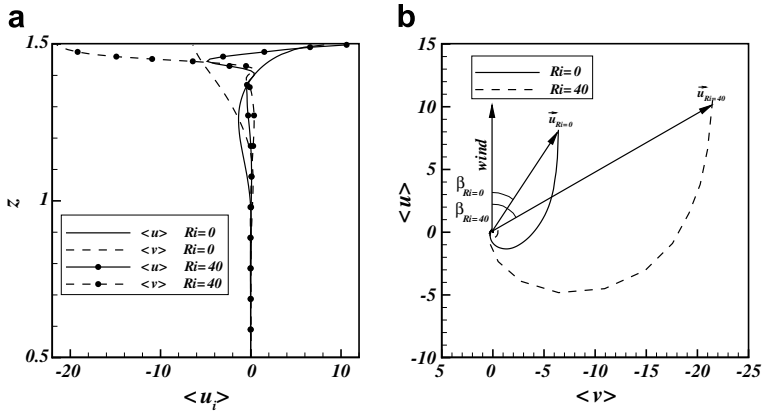

Fig. 3. (a) Vertical profiles of the non-dimensional mean horizontal velocity components. (b) Hodograph of the horizontal components of the mean velocity.

Moreover, large velocity gradients are observed beneath the free surface. As a result, the angle between the wind stress and the velocity vector increases and, in agreement with relevant literature (see for instance Price and Sundermeyer (1999) and Coleman et al. (1992)) the Ekman spiral appears strongly modified (Fig. 3b).

Stratification also affects the elements of the Reynolds stress tensor. Fig. 4a shows the rms of the velocity components, namely the square root of the normal Reynolds stresses. As already observed by Armenio and Sarkar (2002) in the analysis of a strongly stratified turbulent channel flow, stratification affects the normal Reynolds stresses in an anisotropic way. Specifically, the horizontal normal Reynolds stresses are enhanced whereas, the vertical Reynolds stress is strongly inhibited. This is due to the fact that stratification suppresses directly vertical Reynolds stresses as well as the pressure-strain correlation which transfers turbulent kinetic energy (TKE) from the horizontal plane to the vertical direction. As a consequence the TKE produced in the horizontal directions tends to remain confined in the horizontal plane.

The non-dimensional Reynolds shear stresses are shown in Fig. 4b for the two cases studied. We observe that stratification inhibits the amount of vertical mixing of momentum and reduces the thickness of the water column where significant mixing is present. In particular the spanwise-vertical Reynolds stress appears dramatically affected by stratification and this explains the strong increase of the mean spanwise velocity observed in Fig. 3a.

The vertical profiles of the mean density and of its rms are shown in Fig. 5a and b, respectively. In case of neutral flow, the density has to be considered as a passive scalar. From a physical point of view this represents a case where stratification is weak enough that it does not affect the velocity field ($Ri \to 0$).

In the $Ri \to 0$ case we observe that density slowly decreases going up toward the free surface and it appears well mixed in the upper part of the domain. Conversely, in case of strong stratification, the confinement of the mixed layer in the very upper region of the domain causes a strong decrease of the fluid density in the free surface region and the development of a picnocline (layer where the largest density gradient takes place) in a thin region below the free surface. A similar behavior is observed for the density fluctuations, quantified by ρ_{rms} (Fig. 5b): specifically they are very intense and spread over the fluid column in the neutral case, whereas they are confined within a thin region above the picnocline in the stratified case.

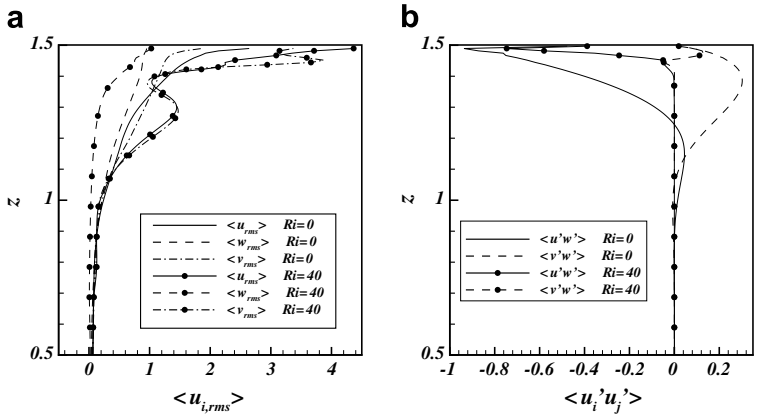

Fig. 4. (a) Vertical profiles of the rms of the velocity components. (b) Vertical profiles of the Reynolds shear stresses.

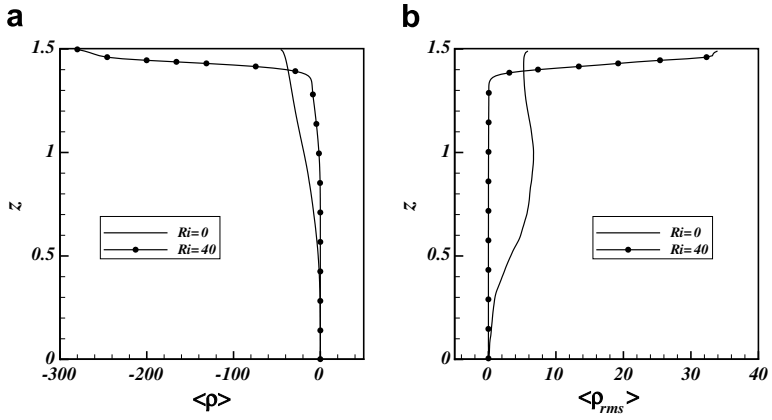

Fig. 5. (a) Vertical profiles of the mean density. (b) Vertical profiles of the density root mean square.

The analysis of the vertical profile of the gradient Richardson number $Ri_g = N^2(z)/S^2(z)$, where $N^2(z) = -g/\rho_0 \mathrm{d}\langle\rho\rangle/\mathrm{d}z$ and $S = \mathrm{d}\langle u\rangle/\mathrm{d}z$, in the stratified case, shows that its value is larger than 0.2 along the whole fluid column. According to Armenio and Sarkar (2002) this indicates that the fluid column is in a *buoyancy dominated* regime, where turbulence is suppressed and internal waves are present in the picnocline region. In Fig. 6 we show the vertical buoyancy flux $\langle\rho' w'\rangle$ which quantifies the attitude to vertical mixing of mass in the fluid column. The $Ri \to 0$ case shows that large vertical buoyancy fluxes are present in the free surface region where active turbulence is present, however noticeable activity is observable along a depth equal to 1.25δ, even larger than the vertical length scale δ.

The presence of strong stratification reduces the vertical buoyancy flux. In particular the maximum value is reduced by more than 20% and, more importantly, the region where appreciable values are recognized remains limited in the free surface region. Counter-gradient buoyancy fluxes are recorded in the region where the picnocline intensifies, and this is a typical feature of the *buoyancy dominated* regime described in Armenio and Sarkar (2002).

Finally Fig. 7 illustrates two iso-density surfaces, respectively in the neutral case and in the $Ri = 40$ one. In the neutral case (Fig. 7a) the iso-surface shows the presence of large mixing spread over a wide range of spatial scales

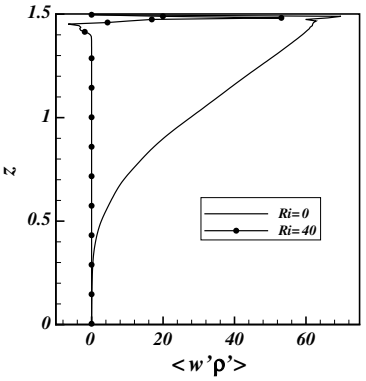

Fig. 6. Vertical profiles of the vertical buoyancy flux.

and extending along the upper part of the water column. Conversely, in Fig. 7b it is possible to see the dramatic inhibition of vertical mixing caused by the stable stratification which is also associated with the presence of internal waves. This destruction of the vertical turbulent structures greatly affects the particle dispersion patterns as it will be shown in the next section.

3.3. Lagrangian particles

The dynamics above observed has a dramatic impact on the dispersion of the buoyant jet. Figs. 8 and 9 offer a 3D

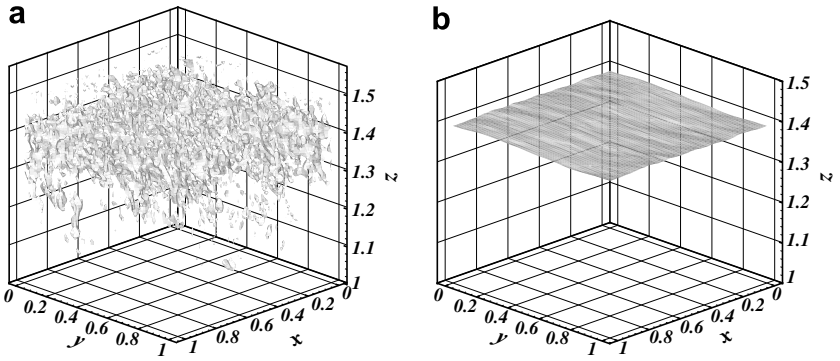

Fig. 7. Iso-density surfaces in the two cases investigated: (a) $Ri \to 0$ and (b) $Ri = 40$. Note the presence of internal waves in the $Ri = 40$ case.

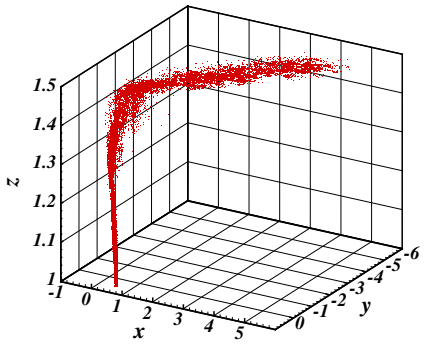

Fig. 8. Three dimensional view of the plume of particles at the final time of simulation $t = 1.1$. Case $Ri \to 0$.

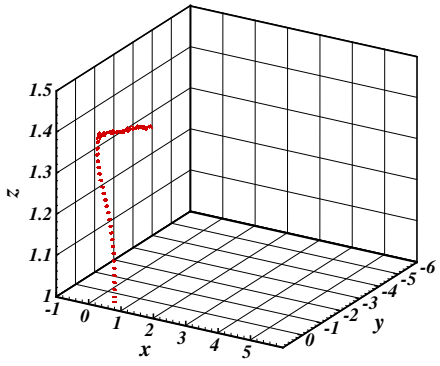

Fig. 9. Three dimensional view of the plume of particles at the final time of simulation $t = 1.1$. Case $Ri = 40$.

view of the plume of particles at $t = 1.10$. In case of neutral flow (Fig. 8) the particulate moves upward along a cylindrical path up to $z = 1.25$, in a region where the level of turbulent fluctuations is very small. Moving upward, the particulate enters a region characterized by the presence of non-zero horizontal velocity components and appreciable turbulent fluctuations, that cause the destruction of the cylindrical structure of the jet and the horizontal spreading of the particulate. This effect is enhanced when the particulate continues to move upward and once it reaches the free surface it is spread horizontally in the flow field.

A very different scenario is observable in the stratified case (Fig. 9). The suppression of turbulence in the region below the picnocline (discussed in the previous section) makes the particulate to travel along a well structured cylindrical path up to the picnocline. Due to the presence of a weak horizontal velocity field and of the Coriolis force, this path undergoes a weak distortion in the region $1.2 < z < 1.35$ still maintaining its own organized structure. However, once the plume reaches the picnocline, it remains confined in that region and oscillates according to a wave-like behavior, due to the presence of internal waves in the fluid column. The confinement of the buoyant jet in the picnocline region has to be attributed to the fact that the particles reach a condition of hydrostatic equilibrium below the free surface, due to the strong reduction of the ambient fluid density (see Fig. 5a). This effect is well known in practical applications (see for example Rubin and Atkinson (2001)) and is well captured by the mathematical model here proposed, which considers an extra-term proportional to the Richardson number in the particle motion equation.

The horizontal displacement and diffusion of the cloud of particulate appear to be inhibited by stratification (see Fig. 10a) for two reasons. The horizontal displacement is strongly reduced because in the stratified case the plume remains entrapped in the picnocline region, well below the free surface, in a region where the horizontal components of the velocity field are small. The horizontal diffusion of the plume is suppressed by stratification due to the inhibition of the turbulent fluctuations in the velocity field.

A lateral view of the plume of particles (Fig. 10b) shows that in the stratified case the jet of particles conserves its shape up to the picnocline; in this region the plume moves horizontally according to the internal waves generated in that region. Conversely, the particles moving in the neutral

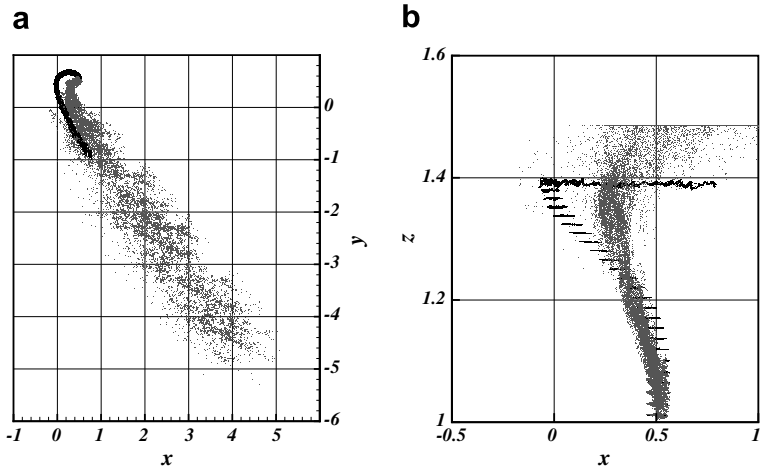

Fig. 10. Two-dimensional views of the plume at $t = 1.1$. Grey particles, $Ri \to 0$; black particles, $Ri = 40$. (a) Top view and (b) side view.

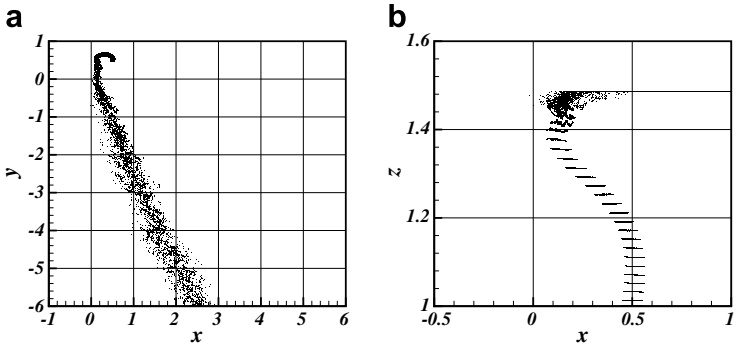

Fig. 11. Two-dimensional views of the plume at $t = 1.1$ evaluated without the Ri term in Eq. (7). a) Top view and b) side view.

flow experience a large horizontal spreading well before reaching the free surface.

With the aim to show the effect of the extra-term proportional to Ri on the dynamics of the plume, we have also run a simulation for the $Ri = 40$ case, not considering the variation of the fluid density in the particle-motion equation, thus omitting the second term of the right hand side of Eq. (7). Fig. 11 shows the top and the lateral view of the plume at $t = 1.1$, when obtained omitting the variable-density term. We observe that if the variation of density is not considered in the particle motion equation, the dynamics of the plume is still affected by the stratification effect on the flow field, in that the strong inhibition of turbulence makes the plume to hold its own cylindrical structure up $z = 1.45$. A spreading occurs above $z = 1.45$ and finally the particles reach the free surface and are spread horizontally according to the velocity field. This happens because the particles are not sensible to the local variation of the ambient density and therefore the entrapment effect below the picnocline is not reproduced. As a consequence the vertical upwelling as well as the horizontal transport are dramatically overpredicted (compare Fig. 11 to Fig. 10).

4. Concluding remarks

In the present paper, the dispersion of a plume of buoyant particles in a stratified wind-driven Ekman layer was investigated. The density ratio herein employed is representative of particles with density comparable with that of the ambient fluid (for example, fresh water particles released into a salty water environment). The analysis was carried out in two different conditions, namely a case of neutral flow and a case of strongly stratified flow. Stable stratification was supplied by incoming heat flux at the free surface of the domain. The study was carried out using LES for the Eulerian phase, whereas the dynamics of the plume of particles was simulated using a Lagrangian technique. In order to make the particles sensitive to the actual fluid density, the particle motion equation was improved and an extra buoyancy term, proportional to the Richardson number, was considered. Because of the Reynolds number considered in our numerical experiment, a wall-model approach was employed, directly imposing the wind stress and the heat flux at the free surface of the domain, not resolving the near-wall structures. The results of the numerical simulations have shown that under stable stratification, the penetration depth of the boundary layer as well as the vertical mixing in the water column decrease. In case of strong stratification, turbulence is almost completely suppressed in the water column and internal waves are observed in the picnocline region. The dispersion of the buoyant jet of particles is dramatically affected by stratification. In the neutral case, once the plume reaches the turbulent region while continuing to go up, it is spread in the horizontal direction by turbulent mixing; afterward, when the particles approach the free surface they are dispersed horizontally according with the local velocity field. In the stratified case, the particles remain entrapped in the picnocline region and are not able to reach the free surface region, characterized by large values of the horizontal velocity components. As a result, both the horizontal displacement and the horizontal spreading of the plume appear strongly inhibited by stratification. In order to check the importance of the extra-term proportional to Ri in the particle-motion equation, we have also run a simulation considering constant ambient density in the particle motion equation. The simulation has clearly shown that neglecting the variation of density leads to a strong overestimation of the vertical as well of the horizontal transport of the plume.

Acknowledgements

The present research has been supported by APAT, under contract: Sviluppo di un modello ad alta definizione per l'analisi della diffusione di getti sommersi in correnti stratificate. The authors wish to express their gratitude to Prof. O. Zikanov who has made available numerical data for the validation of the numerical model.

References

Armenio, V., Fiorotto, V., 2001. The importance of the forces acting on particles in turbulent flows. Physics of Fluids 13, 2437–2440.

Armenio, V., Piomelli, U., 2000. A Lagrangian mixed subgrid-scale model in generalized coordinates. Flow Turbulence and Combustion 65, 51–81.

Armenio, V., Sarkar, S., 2002. An investigation of stably stratified turbulent channel flow using large-eddy simulation. International Journal for Numerical Methods in Fluids 24 (2), 185–214.

Armenio, V., Piomelli, U., Fiorotto, V., 1999. Effect of the subgrid scales on particle motion. Physics of Fluids 11, 3030–3042.

Balaras, E., Benocci, C., Piomelli, U., 1995. Finite-difference computations of high reynolds number flows using the dynamic subgrid-scale model. Theoretical and Computational Fluid Dynamics 7 (3), 207–216.

Bardina, J., Ferziger, J.H., Reynolds, W.C., 1980. Improved subgrid-scale models for large-eddy simulations. AIAA Paper.

Coleman, G.N., Ferziger, J.H., Spalart, P.R., 1990. A numerical study of the turbulent Ekman layer. Journal of Fluid Mechanics 213, 313–348.

Coleman, G.N., Ferziger, J.H., Spalart, P.R., 1992. Direct simulation of the stably stratified turbulent Ekman layer. Journal of Fluid Mechanics 244, 677–712.

Kuerten, J.G.M., 2006. Subgrid modelling in particle-laden channel flow. Physics of Fluids 18 (2), Art. No. 025108.

Lupieri, G., Armenio, V., 2005. An MPI code for Lagrangian dispersion in a turbulent Eulerian field. Science and Supercomputing at Cineca 2005, 378–382.

Marchioli, C., Armenio, V., Soldati, A., 2007. Simple and accurate scheme for fluid velocity interpolation for Eulerian–Lagrangian computation of dispersed flows in 3D curvilinear grids. Computers & Fluids 36 (7), 1187–1198.

Maxey, R., Riley, J., 1983. Equation of motion for a small rigid sphere in a nonuniform flow. Physics of Fluids 26, 883–889.

Price, J.F., Sundermeyer, M.A., 1999. Stratified Ekman layers. Journal of Geophysical Research Space Physics 104, 20467–20494.

Rubin, H., Atkinson, J.F., 2001. Environmental Fluid Mechanics. Marcel Dekker Inc., New York.

Salon, S., Armenio, V., Crise, A., 2005. Large-eddy simulation of an oscillating–rotating turbulent flow. In: Proceedings of the Fourth International Symposium on Turbulence and Shear Flow Phenomena - TSFP4, vol. 2, Williamsburg, VA, USA, pp. 383–388.

Salon, S., Armenio, V., Crise, A., 2007. A numerical investigation of the Stokes boundary layer in the turbulent regime. Journal of Fluid Mechanics 570, 253–296.

Shotorban, B., Mashayek, F., 2005. Modeling subgrid-scale effects on particles by approximate deconvolution. Physics of Fluids 17 (8), Art. No. 081701.

Taylor, J.R., Sarkar, S., Armenio, V., 2005. Large eddy simulation of stably stratified open channel flow. Physics of Fluids 17 (11), Art. No. 11660.

Zang, Y., Street, R.L., Koseff, J.R., 1994. A non-staggered grid, fractional step method for time-dependent incompressible Navier–Stokes equations in curvilinear coordinates. Journal of Computational Physics 114, 18–33.

Zikanov, O., Slinn, D.N., Dhanak, M.R., 2003. Large-eddy simulations of the wind-induced turbulent Ekman layer. Journal of Fluid Mechanics 495, 343–368.